Differential Activity-Driven Instabilities in Biphasic Active Matter

Christoph A. Weber, Chris H. Rycroft, and L. Mahadevan

Phys. Rev. Lett. **120**, 248003 — Published 12 June 2018

DOI: 10.1103/PhysRevLett.120.248003

Differential-activity driven instabilities in biphasic active matter

Christoph A. Weber,[1] Chris H. Rycroft,[1,2] and L. Mahadevan[3,*]

[1] *Paulson School of Engineering and Applied Sciences, Harvard University, Cambridge, MA 02138, USA*
[2] *Mathematics Group, Lawrence Berkeley National Laboratory, Berkeley, CA 94720, USA*
[3] *Paulson School of Engineering and Applied Sciences, Department of Physics, Department of Organismic and Evolutionary Biology, Harvard University, Cambridge, MA 02138, USA*

Active stresses can cause instabilities in contractile gels and living tissues. Here we provide a generic hydrodynamic theory that treats these systems as a mixture of two phases of varying activity and different mechanical properties. We find that differential activity between the phases causes a uniform mixture to undergo a demixing instability. We follow the nonlinear evolution of the instability and characterize a phase diagram of the resulting patterns. Our study complements other instability mechanisms in mixtures driven by differential adhesion, differential diffusion, differential growth, and differential motion.

PACS numbers: 46.32.+x, 81.05.Rm, 47.56.+r, 47.20.Gv

Biological systems are distinguished by the presence of active stresses which affect their properties and alter their stability. For example, active stresses give rise to collectively moving streaks [1] and clusters [2–4], rotating ring, swirl or aster-like patterns [5–9, 53], or the remodelling of cell-to-cell junctions in living tissues [11]. These systems are typically described as a single phase with active stresses that drive the assembly of the constituents and the properties of the phases are typically assumed as liquid-like [12–14] or even gas-like [15–18].

However many active materials cannot be treated as fluids. Examples include cartilage, bone, tissues in early development, and superprecipitated systems such as networks of filaments connected by crosslinks and molecular motors. The presence of activity in these systems drives the macroscopic contraction of gels [9, 19, 53], the compaction of cells during the condensation of cartilage cells [20], the network formation of osteoblasts during skull closure in embryos [21], the formation of furrows and tubes in tissues [22, 23] and causes cellular motility [24, 25]. All these systems are composed of multiple phases with different rheological properties and subject to multiple types of active forcing. This differential activity can cause instabilities in a variety of systems such as chromosome positioning [26], demixing in polydisperse colloidal mixtures [27, 28], and in polythermal mixtures [29]. Thus, we need to go beyond one-component descriptions used to describe isotropic active gels [12, 23–25] and include a more general biphasic description [30, 31]. While recent work has included activity in a poroelastic description [32, 33], the material was assumed to be homogeneous and stable despite active stress generation in one of the phases. Here we relax this assumption of the stability of an active mixture composed of two phases with different activity and different mechanical properties, and ask under what physical conditions an active poroelastic material might contract/condense or disintegrate/fragment.

We start with a consideration of isotropic active systems composed of two immiscible phases, $i = 1, 2$. These systems can be described by a hydrodynamic theory similar to descriptions used for fluid-like biphasic matter [34, 35], or elastic [36] and viscoelastic gels [37, 38]. This theory is valid on length scales above the characteristic pore size of the solid-like phase (Fig. **??**(c)). At the simplest level, activity in our biphasic system is described as an isotropic active stress that acts on each phase which responds to this stress according to its passive mechanical properties which are either fluid or solid-like, respectively. Each phase (i) is described by the hydrodynamic variables of velocity $v_\alpha^{(i)}$, volume fraction $\phi^{(i)}$ and displacement $u_\alpha^{(i)}$ with $\partial_t u_\alpha^{(i)} = v_\alpha^{(i)}$. The overall system is assumed to be incompressible and fully occupied by the two phases, i.e. $\phi \equiv \phi^{(1)} = 1 - \phi^{(2)}$. The fractions of each phase i are conserved, so that $\partial_t \phi^{(i)} = -\partial_\alpha(\phi^{(i)} v_\alpha^{(i)} + j_\alpha^{(i)})$, where $j_\alpha^{(i)}$ denotes a relative flux between the phases with $j_\alpha^{(1)} = -j_\alpha^{(2)} =: j_\alpha$. This relative flux can for example stem from rare unbinding events of components that belong to one of the phases. The resulting unbound components can diffuse and thereby cause an effective diffusive flux of the bound components (see Supplemental Material [39], I). For simplicity, we write $j_\alpha = -D\partial_\alpha \phi$, where D denotes the diffusion constant. The two conservation laws can be equivalently expressed by one transport equation and an incompressibility condition,

$$\partial_t \phi = -\partial_\alpha \left(\phi v_\alpha^{(1)} \right) + D\partial_\alpha^2 \phi \,, \tag{1a}$$

$$0 = \partial_\alpha \left[\phi \, v_\alpha^{(1)} + (1-\phi) \, v_\alpha^{(2)} \right] . \tag{1b}$$

Neglecting osmotic effects and inertia, force balance in

* Corresponding author:lmahadev@g.harvard.edu

each phase implies:

$$0 = \partial_\beta \left(\phi\sigma^{(1)}_{\alpha\beta}\right) - \phi\partial_\alpha p - \mathcal{F}_\alpha \,, \tag{2a}$$

$$0 = \partial_\beta \left((1-\phi)\sigma^{(2)}_{\alpha\beta}\right) - (1-\phi)\partial_\alpha p + \mathcal{F}_\alpha \,, \tag{2b}$$

where $\sigma^{(i)}_{\alpha\beta}$ is the additional stress (beyond the pressure) in each phase, and we have assumed, as in mixture theory [40–42] that this stress is weighted by the respective volume fraction [43]. The pressure p acts as a Lagrange multiplier that ensures the incompressibility condition Eq. (1b). Momentum transfer between the phases is described by a friction force density $\mathcal{F}$. To leading order $\mathcal{F}$ is proportional to the relative velocity of the phases, $\mathcal{F}_\alpha = \Gamma(\phi)(v^{(1)}_\alpha - v^{(2)}_\alpha)$, where $\Gamma(\phi) = \Gamma_0\phi(1-\phi)$ is the friction coefficient between the phases with Γ_0 constant. The dependence of the friction coefficient on volume fraction is a consequence of the condition that hydrodynamic momentum transfer vanishes if one of the phases is absent, i.e. $\mathcal{F} = 0$ for $\phi = 0$ or $\phi = 1$. Finally, we additively decompose the stress into the passive stress $\sigma^{(i),\mathrm{p}}_{\alpha\beta}$ and the isotropic activity $A^{(i)}$,

$$\sigma^{(i)}_{\alpha\beta} = \sigma^{(i),\mathrm{p}}_{\alpha\beta} + A^{(i)}\,\delta_{\alpha\beta} \,, \tag{2c}$$

where the passive stress $\sigma^{(i),\mathrm{p}}_{\alpha\beta}$ characterizes the mechanical properties of each phase. In general, the activity depends on all hydrodynamic variables. For simplicity, we focus on activities that depend on the volume fraction ϕ, $A^{(i)} = A^{(i)}(\phi)$. Eqs. (2) can be rewritten as

$$0 = \partial_\beta \left(\phi\sigma^{(1)}_{\alpha\beta} + (1-\phi)\sigma^{(2)}_{\alpha\beta} - \delta_{\alpha\beta}p\right) \,, \tag{3a}$$

$$0 = \partial_\beta \left(\phi\,\sigma^{(1),\mathrm{p}}_{\alpha\beta}\right) - \frac{\phi}{1-\phi}\partial_\beta \left((1-\phi)\sigma^{(2),\mathrm{p}}_{\alpha\beta}\right) + \left(v^{(2)}_\alpha - v^{(1)}_\alpha\right)\Gamma_0\phi + \phi\,A(\phi)\partial_\alpha\phi \,, \tag{3b}$$

where we define

$$A(\phi) = \left[\frac{A^{(1)}}{\phi} + \frac{A^{(2)}}{1-\phi} + \frac{\mathrm{d}}{\mathrm{d}\phi}\left(A^{(1)} - A^{(2)}\right)\right] \tag{3c}$$

as the *differential activity*. The derivatives of the activity $A^{(i)}$ with respect to ϕ appear because gradients of stress enter the force balance Eqs. (2a) and (2b), while the dependencies on the activity $A^{(i)}$ are a consequence of treating the system as a biphasic mixture, i.e. weighting the stress contributions by the respective volume fractions; see Supplemental Material [39], III for more details on Eq. (3c). The specific form of the activities $A^{(i)}$ depends on the system of interest.

To complete our description we have to select constitutive equations for the passive stress of each phase. Depending on the type of multiphasic system such as physical or chemical gels, tissue mixtures or mixtures composed of active colloids, we may consider solid, fluid or visco-elastic stress-strain or stress-strain-rate relationships. However, to illustrate the generic but multi-phase specific dynamic properties, we restrict ourselves to a simple example of a one dimensional, biphasic mixture composed of a (Kelvin) viscoelastic solid, (s), and a fluid phase, (f), with the constitutive equations:

$$\sigma^{\mathrm{s,p}} = \lambda\partial_x u + \zeta\partial_x v \,, \tag{4a}$$

$$\sigma^{\mathrm{f,p}} = 0 \,, \tag{4b}$$

where the one dimensional solid displacement and velocity are u and $v = \mathrm{d}u/\mathrm{d}t \equiv \dot{u}$; the fluid velocity is given by $-v\phi/(1-\phi)$. In Eq. (4a), λ denotes the Lamé coefficient and ζ is the bulk solid viscosity. The viscous stress in the fluid phase can be approximated to zero since fluid strains are negligible relative to solid strains on length scales above the pore size, and in the systems of interest, the solid viscosity typically exceeds the fluid viscosity by several orders in magnitude [44]. Moreover, an additional fluid viscosity does not affect the occurrence of an instability. Since diffusive transport of constituents in this solid-fluid mixture is expected to be slow compared to solid momentum transport, we consider the limit of small diffusivities and use rescalings of length and time scales not containing the diffusion constant. Specifically, we rescale time and length as $t \to (\zeta/\lambda)\,t$ and $x \to \ell\,x$ with $\ell = \sqrt{\zeta/\Gamma_0}$, so that velocities $v \to v\,\ell\lambda/\zeta$ and the scaled equations read:

$$\partial_t\phi = -\partial_x(\phi\dot{u}) + \tilde{D}\partial_x^2\phi \,, \tag{5a}$$

$$0 = \partial_x\left(\phi\partial_x u + \phi\partial_x v\right) + \phi\tilde{A}(\phi)\,\partial_x\phi - \frac{\phi}{1-\phi}\dot{u} \,. \tag{5b}$$

There are two dimensionless parameters in Eqs. (5), measuring the strength of differential activity, $\tilde{A} = A/\lambda$ and diffusivity, $\tilde{D} = D\Gamma_0/\lambda$.

To understand the stability of a homogenous base state given by $u = u_0$, $\dot{u} = 0$ and $\phi = \phi_0$, we perturb the volume fraction of the phases and the displacement and expand the perturbation in terms of Fourier modes of the form $\propto \mathrm{e}^{\omega t + iqx}$ and linearize the equations above. Calculating the largest growing mode to linear order in diffusivity $\tilde{D}$ and to the fourth order in the wavenumber q gives

$$\Re(\omega_+) \simeq \frac{q^2}{B}\left[-1 + \tilde{A}\phi_0\left(1 - \frac{\tilde{D}\,B}{\tilde{A}\phi_0 - 1}\right)\right] - \frac{q^4}{B^2}\left(\tilde{A}\phi_0 - 1\right) \,, \tag{6}$$

for $\phi_0 \in [0,1]$ and $\tilde{A}\phi_0 > 1$, and where $B = 1/(1-\phi_0)$. We see that there is a long wave length instability with $\Re[\omega_+(q)] > 0$ leading to growth of the homogeneous state on length scales $\gtrsim \ell/\sqrt{B}$ (see Supplemental Material [39], II). The instability is driven by differential activity A which competes with frictional momentum transfer between the phases, and diffusion of displacement, velocity and volume fraction. At the onset of the instability where spatial inhomogeneities in strain are negligible,

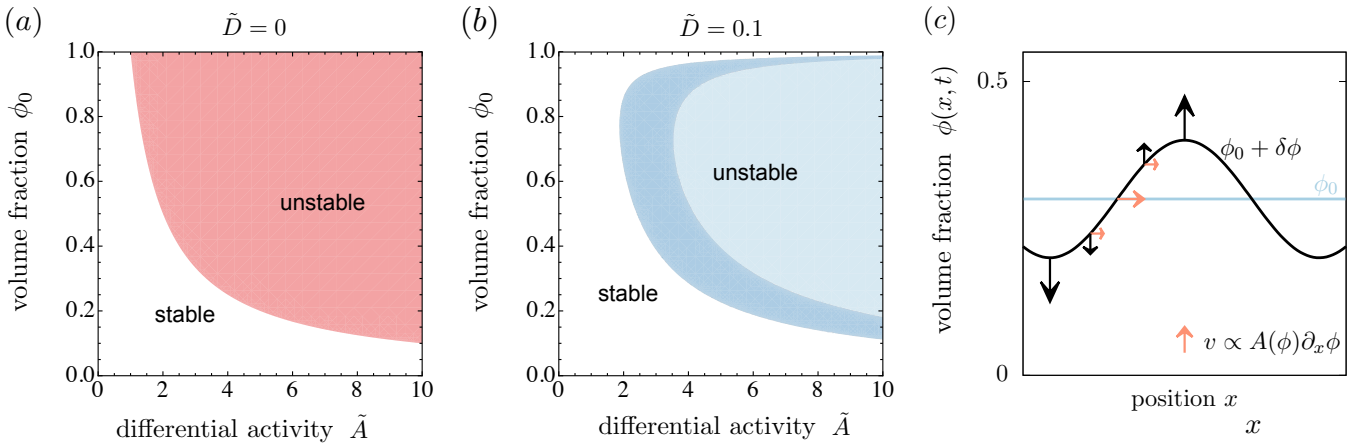

FIG. 1. (a,b) Stability diagrams as a function of volume fraction ϕ and non-dimensional constant differential activity $\tilde{A}$ obtained from the linear stability analysis of Eqs. (3), for different choices of diffusivity (a) $\tilde{D} = 0$ and (b) $\tilde{D} = 0.1$. The colored regions depict $\Re(\omega_+) > 0$. Red indicates an instability where $\Im(\omega_k) = 0$, corresponding to exponential growth, while for dark (light) blue corresponds to $\Im(\omega_k) \neq 0$ for all wave numbers (for a finite band of wavenumbers). (c) Illustration of the instability mechanism driven by differential activity $A(\phi)$. Small perturbations in volume fraction, $\phi_0 \to \phi_0 + \delta\phi$, are amplified since differential activity causes a drift velocity $v = \dot{u}$ that points toward the maximum of a local inhomogeneity of volume fraction. To lowest order in q, this velocity (red horizontal arrows) scales as $v \propto A(\phi)\partial_x\phi$ (Eq. (5b)), further increasing the initial perturbation as indicated by vertical black lines.

long wavelength perturbations in volume fraction are amplified because differential activity causes a solid drift velocity $\dot{u}$ that points toward the maximum of a local inhomogeneity of volume fraction (Fig. 1(c)). This drift scales as $\dot{u} \propto \tilde{A}\partial_x\phi$ to lowest order in q (Eq. (5b). If $A > 0$, the velocity is parallel to the gradient in solid fraction and thus leads a local increase in the solid volume fraction, while it is zero at the local maximum of the inhomogeneity ($\partial_x\phi = 0$). This velocity profile, together with the volume fraction dependent differential activity $A(\phi)$ (Eq. (3c)), may cause the emergence of spikes in the volume fraction around the initial inhomogeneity where $\partial_x\phi$ is largest. These spikes can move inward due to diffusion and amplify the initial perturbation (see movies in Supplemental Material [39],VI).

When the diffusivity vanishes, i.e. $\tilde{D} = 0$, the instability occurs for $\tilde{A} > \tilde{A}_c$ with $\tilde{A}_c = 1/\phi_0$ denoting the critical activity (in real units: $A_c = \lambda/\phi_0$). It is asymmetric with respect to volume fraction and the instability vanishes for $\phi_0 \to 0$ (Fig. 1(a)). The origin of this asymmetry arises from the difference in passive properties of the two phases (Eqs. (4)). Symmetry in volume fraction can for example be restored if both phases are treated as fluids, or as viscoelastic material with equal transport coefficients. The growth rate of the largest growing mode, $\omega_+(q)$, is real for all wavenumbers if $\tilde{D} = 0$ which indicates a non-oscillatory growth of modes (see Supplemental Material [39], IV, for plots of $\omega_k(q)$).

For non-zero diffusivity, the critical activity increases (Eq. (6) and Fig. (2)(c) black line). The term $B = 1/(1-\phi_0)$ connected to viscous transport causes the instability to vanish also at large volume fraction (Fig. 1(b)). In addition, for $\tilde{D} \neq 0$, the growth rate $\omega_k(q)$ can have a non-zero imaginary part. At the transition boundary between the stable and unstable regions, the growth rate is complex for all wavenumbers (dark blue/gray in Fig. 1(b)). However, deep in the unstable regime, the growth rate becomes real for small q but there remains a complex and unstable band of wavenumbers (light blue/gray in Fig. 1(b)). The width of these band of wavenumbers decreases to zero as the diffusivity approaches zero (see Supplemental Material [39], IV).

These two different characteristics in the growth rate obtained from the linear stability analysis indicate that nonlinear evolution of the patterns might also differ in these regimes. To investigate the pattern dynamics we numerically solved the non-linear equations in one and two dimensions; see Supplemental Material [39], III, V,VI for definitions of the used activity functions, details on the numerics, and movies. In one dimension and the limit of zero diffusion, we find that the volume fraction and displacement steadily grow; a behavior that is consistent with a real dispersion relation. In the regime of a purely complex dispersion relation domains of high and low volume fraction exhibit a tendency to synchronously oscillate with a frequency that is roughly determined by the time to diffuse the size of a domain. On longer timescales this oscillating state can spontaneously break the left-right symmetry and the domains collectively move in one direction reminiscent of traveling fronts found in fluid-fluid biphasic matter in the presence of osmotic forces [45]. In contrast, in the mixed case where the dispersion relation is real and complex, the domains of high and low volume fraction separated by sharp interfaces seem to drift while they undergo fusion and break-up events.

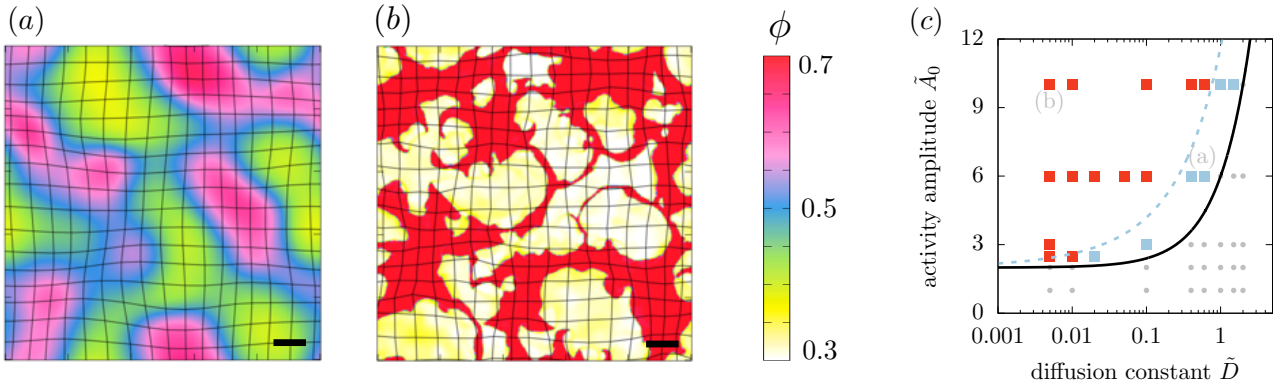

FIG. 2. Patterns and phase diagram in two dimensions obtained from numerically solving Eqs. (3) (see Supplemental Material [39], V,VI for details). (a,b) Two representative snapshots of patterns observed in our active poroelastic model. Black bar depicts the unit length $\ell = \sqrt{\zeta/\Gamma_0}$. Parameters: $\phi_0 = 0.5$, and (a) $\tilde{D} = 0.4$ and $\tilde{A}_0 = 6$, (b) $\tilde{D} = 0.005$, $\tilde{A}_0 = 10$. The black lines depict the displacements of the solid phase. For lower diffusivity, as expected we see sharper boundaries as activity-driven demixing progresses. (c) Phase diagram as a function of non-dimensional diffusivity $\tilde{D}$ and activity amplitude A_0. Squares indicate parameters where the numerical solution shows the emergence of spatial-temporal patterns. Blue/red squares correspond to pattern morphologies shown in (a),(b). The black lines depict the result from the linear stability analysis for Poisson ratio $\nu \approx 0.5$. Parameters above the black curve are linearly unstable; the phase space between the black and blue dashed lines correspond to oscillatory modes for all unstable wavenumbers. In the numerics we considered a specific choice of the activity function (Supplemental Material [39], III) to confine the range of volume fraction ϕ (color bar). This choice ensures the approximate validity of linear elasticity.

In two dimensions we observe similar dynamics. For parameters closer to the transition line where all unstable modes are oscillatory, the system shows a pulsatory type of pattern (Fig. 2(a)). Deep in the unstable regime of the stability diagram (e.g. low $\tilde{D}$ and high activity amplitude A_0) domains with sharp and roughened interfaces drift, split and fuse (Fig. 2(b)). The onset of the instability and the two pattern morphologies determined numerically match the results obtained via linear stability (Fig. 2(c)). However, in two dimensions, we do not observed a collectively moving state. The inter-phase diffusion destabilizes segregated domains on long time-scales leading to oscillatory patterns. In systems with low diffusivities, the spatial standard deviation of displacement and volume fraction steadily increases and saturates once the system reaches its quasi stationary state, while the velocity becomes vanishingly small.

Our study shows how differential activity between the solid and fluid phases that constitute an initially homogeneneous poroelastic medium can drive a mechanical instability. It thus complements instabilities driven by differential size [46], differential shape [47], differential diffusion [48] and differential adhesion [49–51]. More specifically, it generalizes one-component active fluid approaches (e.g. [12]) to two phases that can segregate due to the presence of active stress [32, 33]. Activity and the interactions between the phases can cause an instability leading to patches where solid or fluid matter is enriched. Though we have illustrated the instability for a specific set of constitutive equations (Eqs. (4)) the existence of the instability is generic, i.e. it can occur for any combination of passive mechanical properties of the phases. Furthermore, it predicts that depending on the rate and ability of transport of material and stress in the biphasic material, there will be pulsatile instabilities leading to the assembly, disassembly and drift of solid-like clusters that undergo fusion and fission. Thus, it might thus play an essential role in patterning in cell sorting in tissues, disintegration and macroscopic contractions in super-precipitated systems [9, 19, 53] and patterns in the cellular cortex or the cytoplasm [27, 28]. We hope that it will soon be possible to connect these ideas to concrete experimental realizations with defined types of differential activity and material rheology.

ACKNOWLEDGMENTS

We would like to thank Jakob Löber and Amala Mahadevan for stimulating discussions and Yohai Bar Sinai, David Fronk and Nicholas Derr for insightful comments and feedback on the manuscript. C.A.W. thanks the German Research Foundation (DFG) for financial support. This research was supported in part by the National Science Foundation under Grant No. NSF PHY-1125915. C.H.R. was supported by the Applied Mathematics Program of the U.S. Department of Energy (DOE) Office of Advanced Scientific Computing Research under contract DE-AC02-05CH11231. L. M. was partially supported by fellowships from the MacArthur Foundation and the Radcliffe Institute. L.M. acknowledges partial financial support from NSF DMR 14-20570 and NSF DMREF 15-33985.

[1] V. Schaller *et al.*, Nature **467**, 73 (2010).
[2] C. Dombrowski *et al.*, Phys. Rev. Lett. **93**, 098103 (2004).
[3] H. P. Zhang, A. Be'er, E.-L. Florin, and H. L. Swinney, Proc. Natl. Acad. Sci. USA **107**, 13626 (2010).
[4] C. A. Weber *et al.*, Physical review letters **110**, 208001 (2013).
[5] F. Backouche, L. Haviv, D. Groswasser, and A. Bernheim-Groswasser, Physical Biology **3**, 264 (2006).
[6] A. Kudrolli, G. Lumay, D. Volfson, and L. S. Tsimring, Phys. Rev. Lett. **100**, 058001 (2008).
[7] Y. Sumino *et al.*, Nature **483**, 448 (2012).
[8] V. Schaller *et al.*, Proc. Natl. Acad. Sci. USA **108**, 19183 (2011).
[9] M. Mori *et al.*, Current Biology **21**, 606 (2011).
[10] P. J. Foster, S. Frthauer, M. J. Shelley, and D. J. Needleman, eLife **4**, e10837 (2015).
[11] M. Rauzi, P.-F. Lenne, and T. Lecuit, Nature **468**, 1110 (2010).
[12] J. S. Bois, F. Jülicher, and S. W. Grill, Physical review letters **106**, 028103 (2011).
[13] J. Toner, Phys. Rev. E **86**, 031918 (2012).
[14] J. Prost, F. Jülicher, and J. Joanny, Nature Physics **11**, 111 (2015).
[15] I. S. Aranson and L. S. Tsimring, Phys. Rev. E **71**, 050901 (2005).
[16] E. Bertin, M. Droz, and G. Grégoire, J. Phys. A **42**, 445001 (2009).
[17] C. A. Weber, F. Thüroff, and E. Frey, New Journal of Physics **15**, 045014 (2013).
[18] F. Thüroff, C. A. Weber, and E. Frey, Physical review letters **111**, 190601 (2013).
[19] P. M. Bendix *et al.*, Biophysical Journal **94**, 3126 (2008).
[20] M. Barna and L. Niswander, Developmental Cell **12**, 931 (2007).
[21] J. M. Tabler, C. P. Rice, K. J. Liu, and J. B. Wallingford, Developmental Biology **417**, 4 (2016).
[22] A. C. Martin *et al.*, The Journal of Cell Biology (2010).
[23] E. Hannezo *et al.*, Proceedings of the National Academy of Sciences **112**, 8620 (2015).
[24] R. J. Hawkins *et al.*, Biophysical Journal **101**, 1041 (2011).
[25] A. Callan-Jones and R. Voituriez, New Journal of Physics **15**, 025022 (2013).
[26] N. Ganai, S. Sengupta, and G. I. Menon, Nucleic acids research **42**, 4145 (2014).
[27] J. Stenhammar, R. Wittkowski, D. Marenduzzo, and M. E. Cates, Physical review letters **114**, 018301 (2015).
[28] S. N. Weber, C. A. Weber, and E. Frey, Physical review letters **116**, 058301 (2016).
[29] A. Grosberg and J.-F. Joanny, Physical Review E **92**, 032118 (2015).
[30] E. Moeendarbary *et al.*, Nature materials **12**, 253 (2013).
[31] S. Banerjee and M. C. Marchetti, Soft Matter **7**, 463 (2011).
[32] M. Radszuweit, S. Alonso, H. Engel, and M. Bär, Phys. Rev. Lett. **110**, 138102 (2013).
[33] M. Radszuweit, H. Engel, and M. Bär, PloS one **9**, e99220 (2014).
[34] D. A. Drew, Annual review of fluid mechanics **15**, 261 (1983).
[35] J. P. Keener, S. Sircar, and A. L. Fogelson, SIAM Journal on Applied Mathematics **71**, 854 (2011).
[36] M. Doi, Journal of the Physical Society of Japan **78**, 052001 (2009).
[37] H. Tanaka, Physical review letters **71**, 3158 (1993).
[38] H. Tanaka, Journal of Physics: Condensed Matter **12**, R207 (2000).
[39] See Supplemental Material for videos and more information at http://link.aps.org/supplemental/... .
[40] S. Barry and M. Holmes, IMA journal of applied mathematics **66**, 175 (2001).
[41] S. C. Cowin and L. Cardoso, Mechanics of Materials **44**, 47 (2012).
[42] J. Skotheim and L. Mahadevan, Proceedings of the Royal Society of London A: Mathematical, Physical and Engineering Sciences **460**, 1995 (2004).
[43] The osmotic pressure can also be absorbed into a renormalized activity, which only shifts the transition to larger activities.
[44] M. Spiegelman and D. McKenzie, Earth and Planetary Science Letters **83**, 137 (1987).
[45] N. Cogan, M. Donahue, and M. Whidden, Physical Review E **86**, 056204 (2012).
[46] S. Asakura and F. Oosawa, The Journal of Chemical Physics **22**, 1255 (1954).
[47] L. Onsager, Annals of the New York Academy of Sciences **51**, 627 (1949).
[48] A. M. Turing, Philosophical Transactions of the Royal Society of London B: Biological Sciences **237**, 37 (1952).
[49] P. J. Flory, The Journal of chemical physics **10**, 51 (1942).
[50] M. L. Huggins, The Journal of Physical Chemistry **46**, 151 (1942).
[51] M. S. Steinberg, Journal of Experimental Zoology **173**, 395 (1970).
[52] See Supplemental Material for details, which includes Refs. [53-57].
[53] P. J. Foster, S. Frthauer, M. J. Shelley, and D. J. Needleman, eLife **4**, e10837 (2015).
[54] Specifically, the influence on the numerical integration of the added inertia terms are negligible if $\hat{\rho} = \rho v_0^2/\lambda \ll 1$.
[55] A. J. Chorin, Mathematics of Computation **22**, 745 (1968).
[56] G. R. Dennis, J. J. Hope, and M. T. Johnsson, Computer Physics Communications **184**, 201 (2013).
[57] COMSOL Multiphysics® v. 5.0. www.comsol.com. COMSOL AB, Stockholm, Sweden.